Optimization of X-Ray Prepulse Geometry for Imprint Mitigation in Directly Driven Implosions

Adelyn Carney

Webster Schroeder High School

Advisor: Hans Rinderknecht

Laboratory for Laser Energetics

University of Rochester Rochester

February 2020

1. Abstract

Laser imprint, when laser non-uniformities are imprinted onto the capsule at the beginning of the implosion, is a limiting factor in direct-drive inertial confinement fusion. One method to reduce imprint is x-ray pre-illumination, in which an additional x-ray source is used to "puff up" the outermost layer of the capsule before it is illuminated by the main laser pulse. Positioning metal foils around the capsule and using lasers to heat the foils so they produce x rays is one way to implement this technique. The optimal placement of x-ray prepulse foils was investigated. MATLAB functions were developed to generate foil geometries that correspond to the faces of a tetrahedron, cube, and octahedron, and verify that they satisfy beam clearance requirements. VisRad (J. J. MacFarlane, Journal of Quantitative Spectroscopy and Radiative Transfer **81**, 287 (2003)) models were constructed for selected foil configurations, and viewfactor simulations were run to optimize foil orientation. Three optimized foil configurations were examined: the first configuration optimized uniformity of x-ray distribution on the capsule, the second maximized incident flux by decreasing the foil radius, and the third maximized incident flux by breaking polyhedral symmetry. It was determined that the four-foil geometry would be the most convenient to implement, the six-foil geometry produces the highest mean incident flux with nonuniformity below 10%, and the eight-foil geometry provides the lowest nonuniformity (<8%).

2. Introduction

Because non-renewable energy sources such as coal release carbon dioxide into the atmosphere, a major contributor to global warming, and are projected to run out in only a few centuries, people have been turning to renewable energy sources. The idea of using lasers to initiate a nuclear fusion reaction in a controlled environment was first thought of in the 1960s and first published in 1972 [1, 2]. Since nuclear fusion is both safe and clean (compared to

nuclear fission), much effort has been put into making this idea a reality. Direct-drive inertial confinement fusion [1, 2], studied on the 60-beam OMEGA laser at the Laboratory for Laser Energetics, is one way to achieve it. In this approach, a spherical capsule, which typically has a plastic shell surrounding a layer of frozen deuterium and tritium, is irradiated using high-power laser beams. The capsule implodes, causing extreme temperatures and pressures to be reached. These extreme conditions cause the deuterium and tritium to combine, forming a helium atom and a neutron. If there is enough fusion to further heat the fuel, a chain reaction will occur, known as ignition.

For the best results, the capsule must be irradiated as uniformly as possible. However, uniformity is hard to achieve due to several factors that can worsen over time due to Rayleigh-Taylor instability [3]. One of these factors is laser imprint, in which laser non-uniformities are imprinted onto the surface of the capsule at the beginning of the implosion. As the capsule implodes, the perturbation gets worse, as can be seen in Fig. 1 (taken from Ref. 4). This can destroy the shell of the capsule, reducing capsule performance and the amount of fusion generated. X-ray pre-illumination is one way to reduce laser imprint [5]. In this technique, an additional x-ray source is used to “puff-up” the outermost layer of the capsule before the main laser beams are turned on. This increases the distance between the capsule surface and the region where the laser is initially absorbed, smoothing out the imprint. One way to produce the x-ray prepulse is to position foils around the capsule and hit the foils with laser beams. The foils will then radiate x rays onto the capsule. Figures 2 and 3 support this claim. Figure 2a shows the experimental design when the laser beam directly hits the target, and Fig. 3a shows the result of the laser imprint on the surface of the target when there is no x-ray prepulse. Figure 2b shows the experimental design when the laser beam first goes through a sheet of gold before hitting the target, and Fig. 3b shows the resulting laser imprint on the surface of the

target when there is an x-ray prepulse. When the surface is first pre-illuminated by x rays, a plasma layer is formed that smoothes out the small imprint speckles that are seen in Fig 3a.

In this work, foils will be driven by an OMEGA EP beam transported into the OMEGA target chamber, using a custom optic to split the OMEGA EP beam to focus onto multiple targets, as can be seen in Fig. 4a. Foil configurations made up of four, six, and eight foils were analyzed for optimized uniformity of x rays on the capsule and incident flux. Foil sets will be configured so that the faces of the polyhedra as shown in Fig. 4b correspond to a foil. Section 3 discusses how foil positions were found, including foil constraints, how sets of foils were defined, and how foil geometries and orientations were optimized. Section 4 analyzes the three optimized foil configurations.

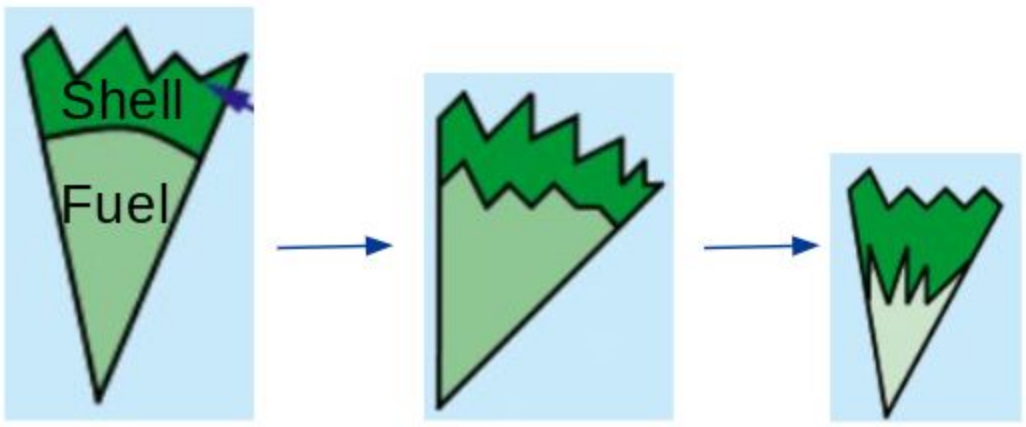

Image from Ref. 4

Figure 1: Series of images showing the effect of laser imprint on an imploding capsule. As time goes on, the perturbations get worse due to Rayleigh-Taylor instabilities.

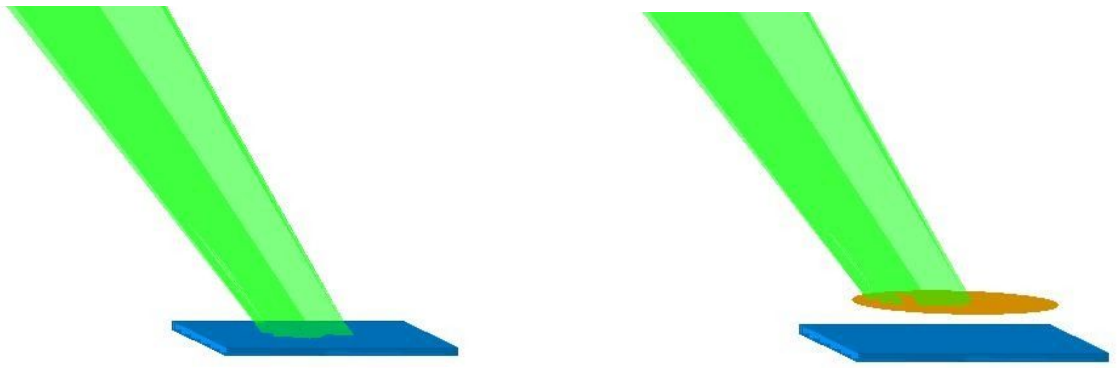

a **b**

Figure 2: Experimental setups to show how laser imprint can be reduced. In (a), the laser beam directly hits the target whereas in (b), the laser beam first goes through a thin gold foil before hitting the target.

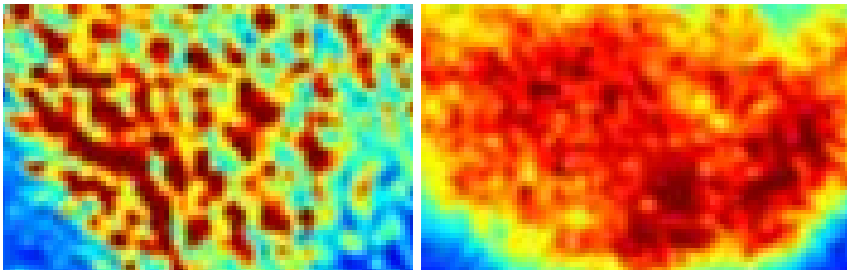

a **b**

Image from Ref. 6

Figure 3: Time resolved x-ray radiography of density modulations from laser imprint from the experiment described in Fig. 2. Color represents mass, with blue showing more mass and red showing less. Where density is greater, more x rays are absorbed. Image (a) shows the imprint left on a surface when the laser hits the surface directly. Image (b) shows the imprint left on a surface when the laser first goes through a thin layer of gold before hitting it. The imprint in image (b) is much smoother because the x-ray prepulse created a layer of plasma near the surface that served as a "buffer" for when the laser hit the surface directly.

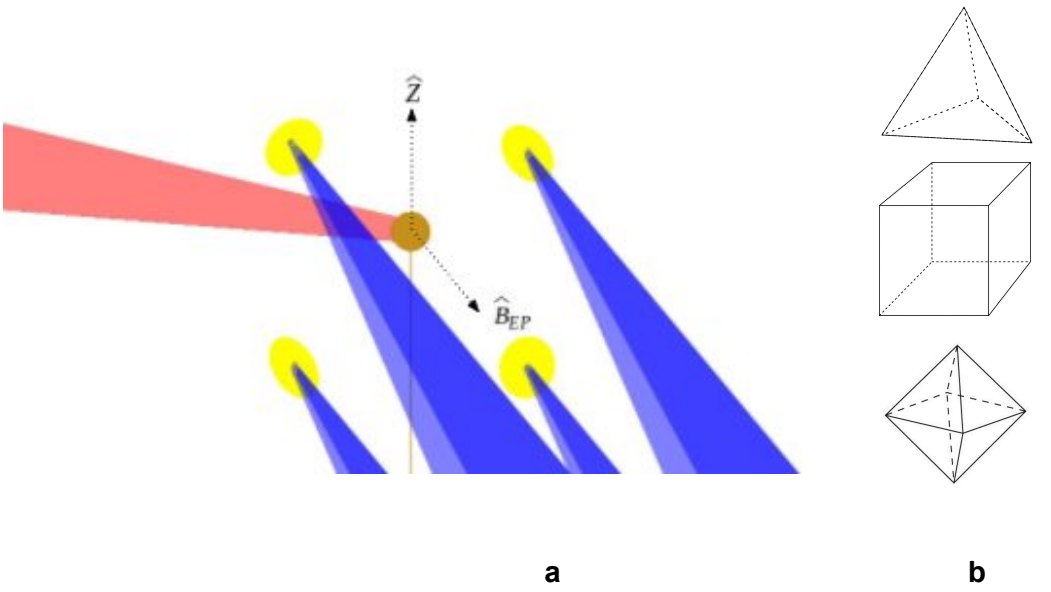

Figure 4: Schematic of foil arrangements. Figure (a) shows the OMEGA EP beam (blue) split up into four beams, each focused on a foil (yellow), and one of the 60 OMEGA laser beams (red) focused onto the capsule (gold). Unit vector, $\hat{B}_{EP}$ is also shown. Figure (b) shows the polyhedral geometry of the foils - the 4-foil geometry will correspond to the faces of the tetrahedron on the top, the 6-foil geometry will correspond to the faces of the cube in the middle, and the 8-foil geometry will correspond to the faces of the octahedron on the bottom.

3. Finding foil positions and orientations

In order to find potential locations where the foils could be placed, constraints on the foils were defined. Then mechanisms were set up to find sets of foils in tetrahedral, cubic, and octahedral geometries, and the most suitable sets of foil geometries were found. The best foil sets were then further analyzed by adjusting the tilt on the foils.

3.1 Foil constraints

Throughout this work, bold indicates vector notation, and the hat symbol, $\hat{}$, indicates a unit vector. For example, the vector **A** = $< A_x\hat{x} + A_y\hat{y} + A_z\hat{z} >$ points in the direction $\hat{A} = \frac{A}{|A|}$.

Constraints on the foils must be satisfied in order for the foils and capsule stalk to not be in the way of any of the OMEGA laser beams and to minimize the risk associated with scattered laser energy. Below are three of these constraints.

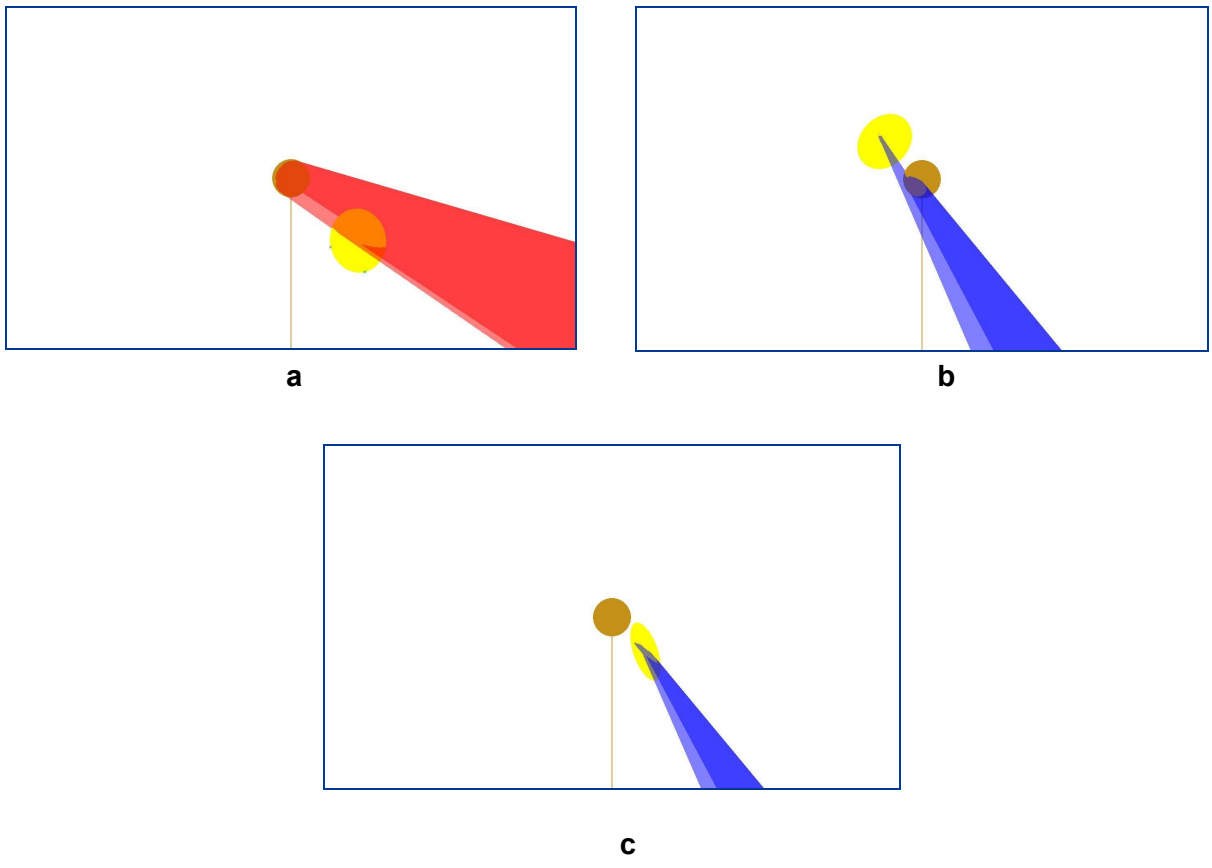

Figure 5: Constraints on the foils. Figure (a) shows an example of when a foil does not clear one of the OMEGA laser beams. Figure (b) shows an example of the target stalk being positioned between an OMEGA EP beam and a foil. Figure (c) shows a large OMEGA EP beam incidence angle.

1) The foils must be clear of all 60 OMEGA laser beams. If the foil is clear of the closest OMEGA beam, then it is clear of all of the beams. An example of a foil not clearing one of the OMEGA laser beams can be seen in Fig. 5a. So, a MATLAB function was generated to loop through all of the OMEGA laser beams and return the Beam ID of the closest beam. The half-angular size is defined as the angle formed by the center of the foil (or beam), the center of

the capsule, and the edge of the foil (or beam). The foil was defined to be clear of the closest beam if the sum of the half-angular sizes of the foil and the beam was less than the angular distance between the center of the foil and the beam. Rotation of the foil will reduce the angular size of the foil, so this condition is an overestimate of the limit which will serve as a safety buffer. The half-angular size of the foil is arctan($\frac{F_r}{r}$) where F_r is the radius of the foil and r is the distance of the foil from the capsule, assuming that the foil is oriented to face the capsule (the worst case). OMEGA beams typically have an f/#, which is the focal length divided by the lens diameter, of 6.65 and a radius at best focus of $R_{spot} \approx 360\ \mu m$. The radius of the OMEGA beam at a distance of r from the focus is approximately $\sqrt{{R_{spot}}^2 + \frac{1}{4}(\frac{r}{6.65})^2}$. Then the half-angular size of the beam at a distance of r from the capsule is approximately arctan($\frac{1}{2}\sqrt{(\frac{R_{spot}}{r})^2 + \frac{1}{4}(\frac{1}{6.65})^2}$). So,

$$\Delta(F,B) \geq \text{arctan}(\tfrac{F_r}{r}) + \text{arctan}(\tfrac{1}{2}\sqrt{(\tfrac{C\,R_{spot}}{r})^2 + \tfrac{1}{4}(\tfrac{1}{6.65})^2}), \qquad [1]$$

where $\Delta(F,B)$ is the angular distance between the center of the foil and the beam and C (≥ 1) is some safety constant, must be satisfied in order for none of the lasers to hit the foil.

2) The capsule stalk cannot be positioned between an OMEGA EP beam and a foil. For this constraint to be satisfied, the foil must be in front of the stalk from the perspective of the beam, the point of closest approach from the beam to the Z (vertical) axis must have a positive Z value (we can assume that the condition that the OMEGA EP beam doesn't hit the capsule has been satisfied), or the beam radius must be smaller than the distance to the stalk at the point on the beam that is closest to the stalk. Fig. 5b shows an example of a foil placed behind the capsule from the perspective of the OMEGA EP beam and as a result, the beam hits the capsule and stalk before it reaches the foil. The points on the beam axis directed at the center

of foil **F** can be defined parametrically as **B**(t) = **F** + t$\widehat{B}_{EP}$, where $\widehat{B}_{EP}$ is the unit vector in the direction the beam comes from (see Fig. 4 for a visual representation). The distance from the beam to the stalk is D(t) = $\sqrt{\widehat{B}_x(t)^2 + \widehat{B}_y(t)^2}$. To find the point of closest approach, $\frac{d(D^2)}{dt}$ = 0 is solved for t, resulting in $t_c = -\frac{F_x\widehat{B}_x + F_y\widehat{B}_y}{\widehat{B}_x^2 + \widehat{B}_y^2}$. The radius of the beam here is $\frac{|t_c|}{2f}$, where *f* is the f-number of the OMEGA-EP beam (f = 6.65). So, the foil is in front of the stalk from the perspective of the beam when

$$t_c < 0.$$

The point of closest approach from the beam to the Z axis has a positive Z value when

$$F_z + t_c\widehat{B}_z > 0.$$

The beam radius is smaller than the closest distance to the stalk when

$$\frac{|t_c|}{2f} < \sqrt{(F_x + t_c\widehat{B}_{EP,x})^2 + (F_y + t_c\widehat{B}_{EP,y})^2} . \qquad [2]$$

The condition is satisfied if any of these are true.

3) The angle of incidence between the OMEGA EP beam and the foil cannot exceed 65°. The laser energy is absorbed best by the foils when they are hit head-on by the laser, so as the angle of incidence increases, less laser energy is absorbed and more scatters, potentially hitting and damaging other equipment in the chamber. This constraint is controlled by the tilt of the foils with respect to the incident laser. A beam-foil coordinate system defined by unit vectors (B_1, B_2, $B_{\parallel}$) was created in which the z-axis ($B_{\parallel}$) is parallel to the direction of the laser beam, the x-axis (B_1) is perpendicular to both the position of the foil with respect to the capsule and the beam direction, and the y-axis (B_2) is perpendicular to the x- and z-axes (see Fig. 6).

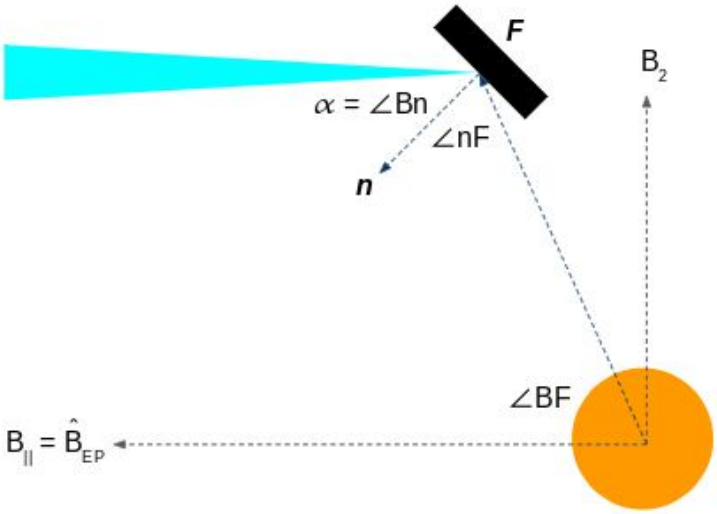

Figure 6: Schematic of OMEGA EP beam (blue), foil (black), and capsule (orange), showing vectors and angles. The unit vector B_1 is directed out of the page.

The orientation angles of the beam with respect to the target chamber axes are polar angle = 116.6° and azimuthal angle = 18°. Let **F** be the position of the foil in cartesian coordinates. Then the new axes can be defined by

$$B_{\parallel} = \widehat{B}_{EP}\,, \qquad [3a]$$

$$B_1 = \frac{F \times B_{\parallel}}{\left| F \times B_{\parallel} \right|}\,, \qquad [3b]$$

and

$$B_2 = B_{\parallel} \times B_1\,, \qquad [3c]$$

where $\times$ is the vector cross product.

Let *p* and *a* be the polar and azimuthal angles of the normal to the foil $\widehat{n}$ with respect to the target chamber. Define $\widehat{n}$ = <x, y, z> to be the cartesian coordinates in the chamber coordinate system when converted from the spherical coordinates <1, *p*, *a*>. Then the normal $\widehat{n}$ is given with respect to the new axes by

$$\widehat{n}(\alpha, \beta) = B_{\parallel} \cos\alpha - (B_1 \sin\beta + B_2 \cos\beta) \sin\alpha \qquad [4]$$

where α is the angle between $\hat{n}$ and B_{II}, and β is the angle between the projection of $\hat{n}$ into the (B_1, B_2) plane and the (-B_2) axis. The tilt of the foil can be defined by two angles,

$$\alpha = \arccos(\hat{n} \cdot B_{\text{II}}) \qquad [5a]$$

and

$$\beta = \arctan\left(\frac{\hat{n} \cdot B_1}{\hat{n} \cdot B_2}\right), \qquad [5b]$$

where α is the in-plane angle (the angle of incidence), β is the out-of-plane angle, and $\cdot$ is the vector dot product. The case where $\beta = 0$ ($\hat{n} \cdot B_1 = 0$) corresponds to the normal $\hat{n}$ lying in the plane of Fig. 6. In order for the angle of incidence between the OMEGA EP beam and the foil to not exceed 65°, α must not exceed 65°. There is no constraint on β. Fig. 5c shows how the α limit makes it difficult to direct the x rays onto the capsule when it has a small $\angle BF$ (from Fig. 6).

3.2 Defining and Generating Sets of Foils

Each set of foil locations can be defined by four parameters, r, θ, ϕ, and η, where r, θ, and ϕ define the position of the first foil, F_1, in spherical coordinates, and η defines the rotation of the remaining foils about the F_1 axis. To determine the positions of the other foils from these four parameters, an axis parallel ($\hat{Z}'$) and axes perpendicular ($\hat{X}'$, $\hat{Y}'$) to F_1 must be defined. $\hat{Z}'$ is a unit vector parallel to F_1, which is defined by

$$\hat{Z}' = \frac{<F_{1x}, F_{1y}, F_{1z}>}{F_{1r}}, \qquad [6]$$

where $F_{1r} = \sqrt{F_{1x}^2 + F_{1y}^2 + F_{1z}^2}$ is the distance of the first foil from the capsule.

To get the perpendicular vectors, a reference vector must be chosen. If <0, 0, 1> is the reference vector, then the perpendicular vectors can be defined as

$$\hat{X}' = \frac{<0, 0, 1> \times \hat{Z}'}{\left| <0, 0, 1> \times \hat{Z}' \right|} \qquad [7]$$

And

$$\widehat{Y}' = \widehat{Z}' \times \widehat{X}'. \qquad [8]$$

If F_1 is parallel to <0, 0, 1>, then $\widehat{X}'$ = <1, 0 ,0>, and $\widehat{Y}'$ = <0, 1, 0>.

The position of foil *j* in the tetrahedral, cubic, and octahedral geometries with a rotation η about the F_1 axis can be written as

$$F_j = F_{1r}[(T_{jx}\cos\eta + T_{jy}\sin\eta)\widehat{X}' + (T_{jy}\cos\eta - T_{jx}\sin\eta)\widehat{Y}' + T_{jz}\widehat{Z}']. \qquad [9]$$

The coefficients T_{ji} are defined in Table 1.

Geometry	*j*	T_{jx}	T_{jy}	T_{jz}
Tetrahedron	1	0	0	1
	2	$\sqrt{8/9}$	0	-1/3
	3	$-\sqrt{2/9}$	$\sqrt{2/3}$	-1/3
	4	$-\sqrt{2/9}$	$-\sqrt{2/3}$	-1/3
Cube	1	0	0	1
	2	1	0	0
	3	0	1	0
	4	-1	0	0
	5	0	-1	0
	6	0	0	-1
Octahedron	1	0	0	1
	2	$\sqrt{2/3}$	$\sqrt{2/9}$	1/3
	3	$-\sqrt{2/3}$	$\sqrt{2/9}$	1/3
	4	0	$-\sqrt{8/9}$	1/3
	5	0	$\sqrt{8/9}$	-1/3
	6	$\sqrt{2/3}$	$-\sqrt{2/9}$	-1/3
	7	$-\sqrt{2/3}$	$-\sqrt{2/9}$	-1/3
	8	0	0	-1

Table 1: Locations of vertices for unit polyhedrons where F_1 *= (0,0,1).*

3.3 Process to find optimal foil geometries

The goal of this study was to find a foil geometry that maximizes mean x-ray intensity on the capsule as well as uniformity. VisRad [7], a view factor code, was used to simulate the radiation flux onto a capsule for each foil geometry. The x-ray uniformity was assessed by calculating the ratio of the incident flux standard deviation to the mean incident flux. Ease of implementation should also be taken into account in the future. So, even though an 8-foil geometry will yield higher uniformity than a 4-foil geometry, it is possible that the 4-foil geometry will be chosen over an 8-foil geometry because it is more practical to field 4 foils than 8. Some actions improved one of these parameters while worsening others, so foil geometries were sought that had a balance between these parameters.

For example, putting the foils closer to the capsule generally increased their x-ray intensity and uniformity. However, this wasn't always the case. For the tetrahedron, since there were only four foils to irradiate the capsule, if the foils got too close, uniformity decreased, contrary to what happened with the cubic and octahedral geometries.

At a given foil-to-capsule distance, the maximum flux was limited by the smallest value of the angle ∠BF (see Fig.6 for these angles) within each set of foils. Since there is an upper limit on ∠Bn (65°), the foil with the smallest ∠BF necessarily has the largest ∠nF, and therefore limits the incident flux on the capsule. The minimum value of ∠BF was found for each set of foils, and the set with the largest minimum value was expected to produce the largest x-ray flux. The largest possible ∠BF was constrained by geometry, and was 70.5° for the tetrahedron and 54.7° for the cube and octahedron. However, due to the constraints described in Section 3.1, these largest possible minimum ∠BF 's could not be achieved in practice. The largest minimum ∠BF that were found were in the 50°s for the tetrahedron and in the 40°s for the cube and octahedron.

A MATLAB function was written to randomly generate sets of foils for each foil geometry given a distance between the foils and the capsule. So, a distance between the foils and the capsule and the number of generated sets of foils that was to be returned would be input into the function, and foil sets with the θ, Φ, and η values along with the smallest ∠BF were returned. In general, the goal was to minimize the distance between the foils and the capsule while also retaining a large, smallest ∠BF. The best sets of foils found for each foil geometry by this random generator were then put into VisRad.

To maximize the smallest ∠BF, an iterative MATLAB function was written to return the range of θ, Φ, or η values (defined in Section 3.2) for a specific foil geometry that satisfied all of the constraints given a foil-to-capsule distance and two of the three parameters, θ, Φ, and η . For example, r, θ, and Φ would be input and ranges, to the nearest hundredths place, of η values that satisfied all of the constraints were output. The previous η value would then be replaced by the value in that output range that produced the largest, smallest ∠BF. This was then done with the other two parameters, θ and Φ: r, Φ, and η would be input and ranges, to the nearest hundredths place, of θ that satisfied all of the constraints were output, and the previous θ value would then be replaced by the value in that output range that produced the largest, smallest ∠BF. Likewise, r, θ, and η would be input and ranges, to the nearest hundredths place, of Φ that satisfied all of the constraints were output, and the previous Φ value would then be replaced by the value in that output range that produced the largest, smallest ∠BF. Starting from a randomly selected foil configuration defined by the four parameters (r, θ, Φ, η) that satisfied the conditions, ranges for θ, Φ, and η were found, and the previous θ, Φ, and η values were replaced by the values in that range that produced the largest, smallest ∠BF. Then the distance between the foils and the capsule would be increased, and this process would be

repeated until the smallest ∠BF was as large as possible while still fulfilling the clearance conditions described in Section 3.1.

3.4 Normal vector optimization

The tilts on the foils were varied in VisRad to optimize intensity and uniformity. The same beam-foil coordinate system was used as in Section 3.1. The normal vector $\hat{n}(\alpha, \beta)$ defined in Eq. (4) can be used in VisRad by converting $\hat{n}$ shown in Fig. 6 to spherical coordinates, (r, polar, azimuthal) with respect to the target chamber axes and inputting the polar and azimuthal angles. A MATLAB function was written that returns the polar and azimuthal angles given the coordinates of the foil and its α and β.

For foils with a small angle $\angle BF$, it is harder for x rays to reach the capsule. So to start, the foil with the smallest $\angle BF$ had its tilt set. α was set to 65°, the maximum tilt allowed in the target chamber, and β was set to 0°. This would maximize the amount of x rays generated by that foil that would be directed towards the capsule since this foil was the limiting factor for the foil set in terms of x-ray intensity.

The alphas and betas of the other foils were determined by manual iteration. The α and β of the other foils were initially set to 65° and 0°, respectively. Then the α and/or β of one of the foils was changed by a small amount. The simulation was then run. If nonuniformity, which was calculated by dividing the standard deviation by the mean incident flux, decreased, the tilt was moving in the right direction and it was further changed in that same direction. If nonuniformity increased, the tilt was changed in the opposite direction. The tilt on each foil was altered a little bit before moving onto the next foil. The foils' tilts were optimized in a rotating pattern, excluding the foil with the smallest $\angle BF$. No foil was altered too much at once. In the end, each foil's tilt was altered multiple times with the goal of maximizing uniformity. This procedure did not guarantee that an optimal radiation intensity and uniformity was reached for each foil geometry.

However, by inspection, reasonable illumination symmetry was achieved for all geometries, as described in the next section.

4. Optimized foil geometries

Three approaches were taken to optimize foil geometries. The first approach optimized x-ray uniformity on the capsule. The other two approaches maximized incident flux by decreasing the distance between the foils and the capsule, either by decreasing the radius of the foils or by breaking the polyhedral symmetry.

4.1 Optimized Uniformity with Foil Radius of 0.8 mm

This approach worked on decreasing the nonuniformity of the x-ray distribution on the capsule by finding good foil geometries as described in section 3.3 and then optimizing the normal vector through the process described in section 3.4. The results can be found in Table 2. Incident flux and uniformity can be visually compared between the three foil geometries in Fig 7. (The same total beam power, which is energy per unit time of a beam, was used for the 4-foil, 6-foil, and 8-foil geometry in all three scenarios. In this simulation, 1 TW of total beam power was used and a conversion efficiency of 60% into x rays was assumed.) The cubic geometry produced the highest mean incident flux, while the octahedral geometry produced the most uniform distribution of x rays onto the capsule. The octahedral geometry had the lowest mean incident flux because this geometry utilized the highest number of foils so in order to satisfy all of the constraints, it needed a bigger r value, decreasing x-ray intensity. However, this geometry had the best uniformity because its large number of foils allowed it to irradiate the capsule the most evenly.

	(r, theta, phi, eta) (r in mm and θ, Φ, and η in °)	Mean incident flux (TW/ cm^2)	$\frac{standard\ deviation}{mean}$
Tetrahedron	(9.2, 64.4, 340.6, 97.9)	0.036	0.096
Cube	(6.6, 56.8, 336.6, 96.3)	0.047	0.095
Octahedron	(11.4, 117.5, -125.8, 69.9)	0.014	0.08

Table 2: Location, mean incident flux, and uniformity measure for the most uniform tetrahedral, cubic, and octahedral foil geometries found. Of these three, the cubic geometry had the highest mean incident flux, and the octahedral geometry had the lowest. The octahedral geometry was also the most uniform, although all had uniformity better than 10%.

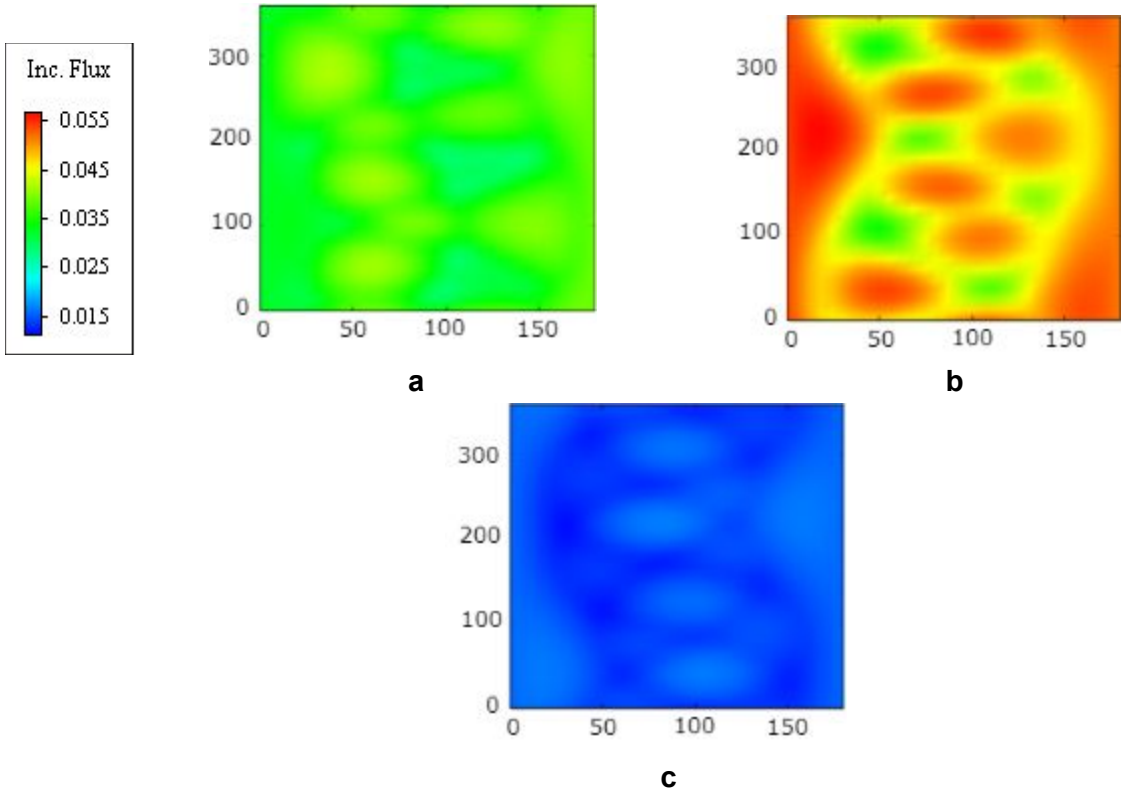

Figure 7: Incident flux plots (TW/cm^2) versus location on the capsule surface for the (a) tetrahedral, (b) cubic, and (c) octahedral foil geometries with θ on the horizontal axis (in degrees) and Φ on the vertical axis.

4.2 Maximized Incident Flux by Decreasing Radius

This approach used the foil positions found in Section 4.1 as the baseline. The radii of the foils were decreased, allowing them to sit closer to the capsule. Since uniformity decreased as the foils got closer to the capsule for the tetrahedral foil geometry, the cubic and octahedral foil geometries were the only polyhedra analyzed using this technique. The radii of the foils were decreased from 0.8 mm to 0.5 mm, although it is unknown how small the foils can actually get. (Ease of implementation and practicality must be taken into account.) Then the same approach as used in Section 4.1 was used to maximize uniformity. The results can be found in Table 3. The increase in incident flux intensity can be seen visually in Fig. 8, with a 61% increase for the cubic geometry and a 74% increase for the octahedral geometry. Uniformity improved as well but not by much.

	(r, theta, phi, eta) (r in mm and θ, Φ, and η in °)	Mean incident flux (TW/ cm^2)	$\frac{standard\ deviation}{mean}$
Cube	(5.2, 56.8, 336.6, 96.3)	0.076	0.092
Octahedron	(8.7, 1, 354, 82)	0.025	0.079

Table 3: Location, mean incident flux, and uniformity measure for the cubic and octahedral foil geometries found that maximized incident flux by decreasing the foil radius from 0.8 mm to 0.5 mm. The mean incident flux increased greatly for both geometries with a 61% increase in the cubic geometry and a 74% increase in the octahedral geometry while maintaining almost the same uniformity. The cubic geometry still had the highest mean incident flux, and the octahedral geometry was still the most uniform.

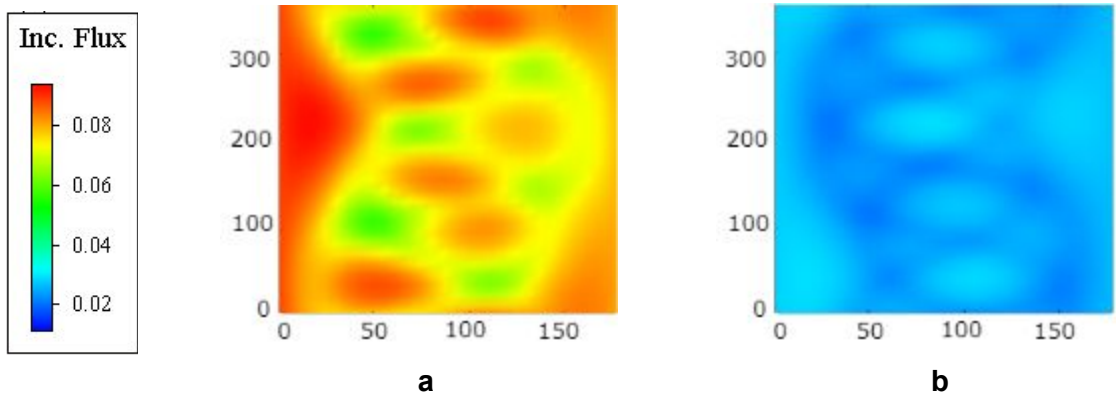

Figure 8: Incident flux plots (TW/cm^2) versus location on the capsule surface for the (a) cubic geometry and (b) octahedral geometry with θ on the horizontal axis and Φ on the vertical axis after the foil radius was decreased from 0.8 mm to 0.5 mm.

4.3 Maximized Incident Flux by Breaking Symmetry

This approach also used the foil positions found in Section 4.1 as a baseline. The radii of the foils was held at 0.8 mm in this approach, the same as in Section 4.1. From there, the position of any foil that was so close to any of the OMEGA beams that the distance between the foil and capsule couldn't be decreased any more was moved slightly away from whichever beam it was closest to. This allowed for the distances between the foils and the capsule to be decreased even more, increasing the incident flux but also increasing nonuniformity. The process of breaking polyhedral symmetry and decreasing the distance between the foils and the capsule was continued until $\frac{standard\ deviation}{mean}$ equalled 0.1. The results can be found in Table 4. The change in incident flux intensity and uniformity can be seen visually in Fig. 9. When Sections 4.1 and 4.3 are compared, a dramatic increase in incident flux intensity can be seen for both geometries. The foils for the cubic geometry were able to get slightly closer to the capsule (the r value decreased from 6.6 mm to 5.7 mm), while the foils for the octahedral geometry were able to get much closer to the capsule (the r value decreased from 11.4 mm to 6.5 mm). This allowed for the cubic geometry to experience a 34% increase in incident flux and

the octahedral geometry to experience a large, 273% increase. Nonuniformity increased slightly for both, with a 5% increase for the cubic geometry and a 25% increase for the octahedral geometry.

	(r, theta, phi, eta) (r in mm and θ, Φ, and η in °)	Mean incident flux (TW/ cm^2)	$\frac{standard\ deviation}{mean}$
Cube	(5.7, 56.8, 336.6, 96.3)	0.063	0.1
Octahedron	(6.5, 1, 354, 82)	0.053	0.1

Table 4: Location, mean incident flux, and uniformity measure for the cubic and octahedral foil geometries found that maximized incident flux by breaking the symmetry of the foils while keeping $\frac{standard\ deviation}{mean}$ *below 0.1. (The (x, y, z) coordinates for each foil don't match exactly with the given (r, theta, phi, eta) values because their positions were moved in order to avoid the beams.) This approach increased the incident flux by 34% for the cube and 273% for the octahedron.*

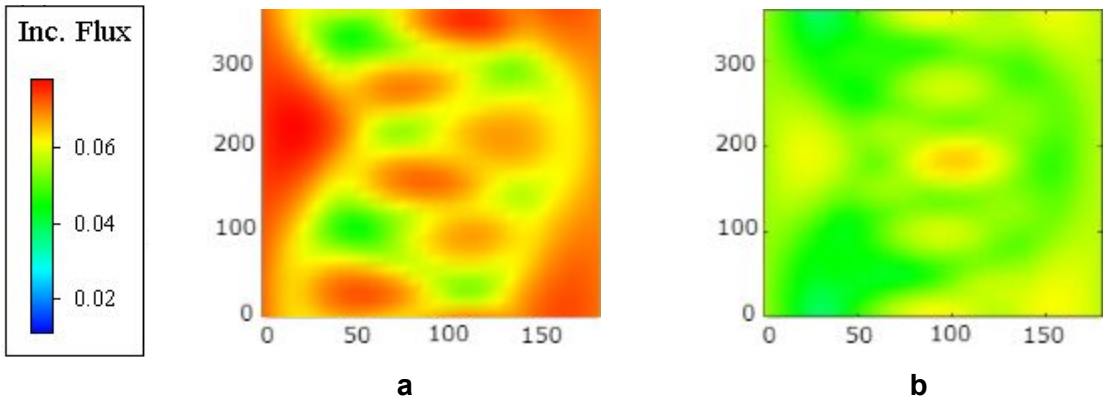

Figure 9: Incident flux plots (TW/cm^2) versus location on capsule surface for the (a) cubic geometry and (b) octahedral geometry with θ on horizontal axis and Φ on vertical axis after polyhedral symmetry was broken.

5. Conclusion

In direct-drive inertial confinement fusion, it is important that the capsule be irradiated as uniformly as possible in order to maximize the amount of fusion generated during the implosion.

Laser imprint is one cause of capsule nonuniformities. This project explored the x-ray pre-illumination technique in which metal foils are heated to produce x rays onto the capsule before the main lasers are turned on. MATLAB functions were written to find optimal foil locations; these foils were then put into VisRad where foil locations and tilts were analyzed in order to optimize the incident flux and uniformity on the capsule. Foil positions were found three different ways: the first optimized uniformity, the second maximized incident flux by decreasing the radii of the foils to allow the distance between the foils and the capsule to be decreased, and the third allowed the foils to come closer to the capsule by breaking polyhedral symmetry. The six-foil geometry produced the highest mean incident flux in all three cases with nonuniformity below 10%. The eight-foil geometry provided the lowest asymmetry (<8%) at the expense of a greatly reduced incident flux. However, the four-foil geometry would be easiest to implement. Future work includes realistic mounting for the foils, calculations of absorbed flux using real x-ray spectra, and ultimately experimental tests.

6. Acknowledgements

I would like to thank my advisor, Dr. Hans Rinderknecht, for his guidance throughout my project. I couldn't have done it without his patience and endurance. I would also like to thank Dr. Jonathan Peebles for sharing his experimental results with me to assist with my project report. Lastly, I would like to thank Dr. Stephen Craxton for making possible this once-in-a-lifetime opportunity of working in this world-renowned laboratory.

7. References

1. J. Nuckolls, L. Wood, A. Thiessen, and G. Zimmerman, "Laser compression of matter to super-high densities: Thermonuclear (CRT) applications," Nature, **239**, 139 (1972).
2. R.S. Craxton et al., "Direct-Drive Inertial Confinement Fusion: A Review," Physics of Plasmas **22**, 110501 (2015).

3. D.H. Sharp, “An Overview of Rayleigh-Taylor Instability,” Physica D. **12**: 3-18 (1948).
4. O. Willi “Lecture 2: Symmetry issues”, Institut für Laser - und Plasmaphysik
5. M. Nishikino, et al., “Imprint reduction in a plasma layer preformed with x-ray irradiation,” Phys. Plasmas **9**, 1381 (2002).
6. J. Peebles, private communication, Sept 2019.
7. J. J. MacFarlane, “VISRAD – A 3-D view factor code and design tool for high-energy density physics experiments,” Journal of Quantitative Spectroscopy and Radiative Transfer 81, 287 (2003).